Inhibition of the Ras-Net (Elk-3) Pathway by a Novel Pyrazole that Affects Microtubules

Christine Wasylyk,[1] Hong Zheng,[1] Christelle Castell,[2] Laurent Debussche,[2] Marie-Christine Multon,[2] and Bohdan Wasylyk[1]

[1]Institut de Génétique et de Biologie Moléculaire et Cellulaire, Centre National de la Recherche Scientifique/Institut National de la Sante et de la Recherche Medicale/Université Louis Pasteur, Illkirch Cedex, France and
[2]Sanofi-Aventis, Oncology Therapeutic Department, Vitry-sur-seine, France

Abstract

Net (Elk-3/SAP-2/Erp) is a transcription factor that is phosphorylated and activated by the Ras–extracellular signal-regulated kinase (Erk) signaling pathway and is involved in wound healing, angiogenesis, and tumor growth. In a cell-based screen for small molecule inhibitors of Ras activation of Net transcriptional activity, we identified a novel pyrazole, XRP44X. XRP44X inhibits fibroblast growth factor 2 (FGF-2)–induced Net phosphorylation by the Ras-Erk signaling upstream from Ras. It also binds to the colchicine-binding site of tubulin, depolymerizes microtubules, stimulates cell membrane blebbing, and affects the morphology of the actin skeleton. Interestingly, Combretastin-A4, which produces similar effects on the cytoskeleton, also inhibits FGF-2 Ras-Net signaling. This differs from other classes of agents that target microtubules, which have either little effect (vincristine) or no effect (docetaxel and nocodazole) on the Ras-Net pathway. XRP44X inhibits various cellular properties, including cell growth, cell cycle progression, and aortal sprouting, similar to other molecules that bind to the tubulin colchicine site. XRP44X has the potentially interesting property of connecting two important pathways involved in cell transformation and may thereby represent an interesting class of molecules that could be developed for cancer treatment. [Cancer Res 2008;68(5):1275–83]

Introduction

The Ras pathway is an attractive target for the development of chemotherapeutic intervention. Human cancers frequently have mutations in components of the Ras pathway, which result in uncontrolled cell growth that is freed from regulation by environmental signals (1–3). Ras links signals emanating from receptor tyrosine kinases to downstream effectors, such as extracellular signal-regulated kinase 1 (Erk-1) and Erk-2, that phosphorylate effectors, such as transcription factors of the Ets family (4). Ets proteins are implicated in malignant transformation, and interestingly, *ets* gene fusions are frequently rearranged in human malignancies (5–7). We have focused on one of the Ets factors that is regulated by Erk phosphorylation: Net (also called Elk-3).

Net is an interesting downstream target of the Ras pathway, which has an important role in physiologic and pathologic processes, including wound healing, cell migration, angiogenesis, and tumorigenesis (8–11). Net can be considered, thus, as a relevant target for drug screens. Net, together with Elk-1 and Sap-1, forms the ternary complex transcription factor subfamily (TCF), which is notably known for their participation in the early response of quiescent cells to growth factor stimulation (review ref. 12). Net is a strong transcriptional repressor under basal conditions due to the activities of two repressor domains, the NID and the CID (Fig. 1*A*). Activation of the growth factor–Ras–mitogen-activated protein kinase (MAPK) pathway leads to Erk binding to the D and F boxes and phosphorylation of Net on critical amino acids, such as Ser^{363} in human Net, which converts the C domain into an efficient transcription activation domain. A phosphorylated-specific antibody that recognizes this important modification has been developed and shown to specifically stain transformed cells in various human tumors, including prostate cancer (10).

In this study, we used the Ras-activated COOH terminal domain of Net in a cell-based high-throughput screen to identify inhibitors of the activity of the C-domain linked to a heterologous DNA-binding domain and reporter construct. One of the inhibitors, XRP44X, turned out to be a microtubule-depolymerizing agent that interacts with the colchicine-binding site of tubulin. Microtubules are dynamic components of the cytoskeleton, which have a number of important functions related to movement of both organelles during interphase and chromosomes during mitosis. Microtubules are important targets for anticancer therapy, and clinically successful microtubule "poisons" include the taxanes and *Vinca* alkaloids (review refs. 13–15). Microtubules are composed of heterodimers of α-tubulin and β-tubulin. Tubulin-binding drugs can be classified according to the sites on tubulin they bind. Most of the successful drugs target the taxane-binding and *Vinca*-binding sites, and agents that target the colchicine-binding site are being developed [e.g., combretastatin prodrugs, such as combretastatin A4 (CA4)–phosphate and combretastatin-serine (AVE8062)]. Tubulin-binding drugs can also be classified according to whether they stabilize microtubules and stimulate polymerization (e.g., taxanes) or destabilize microtubules and inhibit polymerization (e.g., Vinca alkaloids, nocodazole, and combretastatins). The primary antineoplastic activity of the drugs is thought to result from the failure of cells to segregate chromosomes during mitosis. However, at least part of their activity could result from nonmitotic effects in interphase cells. These additional effects may help explain some of the differences between the activities of microtubule "poisons" and may help in the development of improved drugs. In particular, drugs that target the colchicine domain, such as combretastatins, act as vascular-disrupting agents.

Note: Supplementary data for this article are available at Cancer Research Online (http://cancerres.aacrjournals.org/).

Requests for reprints: Bohdan Wasylyk, Institut de Génétique et de Biologie Moléculaire et Cellulaire, Parc d'Innovation, 1 Rue Laurent Fries, BP 10142, 67404 Illkirch Cedex, France. Phone: 33-3-88-65-34-11; Fax: 33-3-88-65-32-01; E-mail: boh@igbmc.u-strasbg.fr.

doi:10.1158/0008-5472.CAN-07-2674

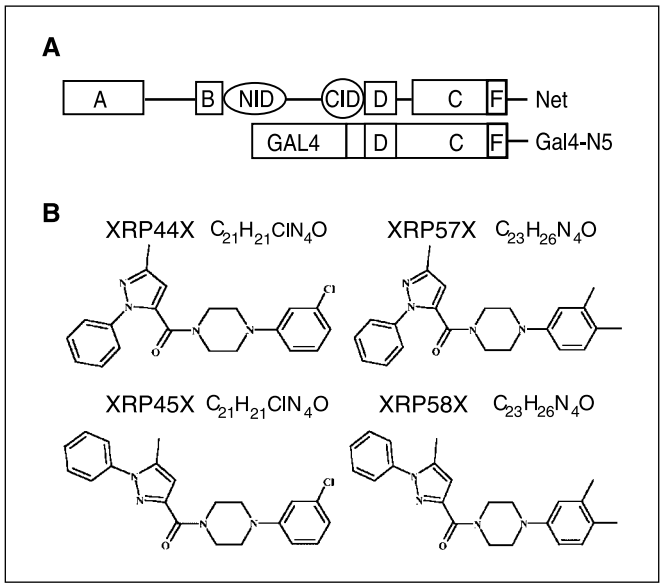

Figure 1. *A,* structure of full-length Net and its Ras-responsive COOH terminal activation domain fused to the Gal4 DNA-binding domain (Gal4-Net). *B,* names, chemical formulas, and structures of piperazinylcarbonyl-pyrazole derivatives isolated in the screens and their regioisomers used as controls.

Interestingly, XRP44X was found to have many properties in common with CA4, such as antimitotic and vasculature-disrupting effects (16). Here, we report that it also inhibits Net activity and phosphorylation by its negative effects on the Ras signaling pathway, a property shared with CA4 and but not with docetaxel and nocodazole. It also inhibits the growth of transformed cells in culture and angiogenesis in an *ex vivo* assay of endothelial cell sprouting. Our studies provide evidence for a novel pathway for regulation of Ras-MAPK signaling and identify a new molecule that may be useful for the development of cancer therapy.

Materials and Methods

For details, see Supplementary Materials and Methods.

Recombinants. Net, Gal4-N6, Gal4-N5, 8xPal-TK-Luc, Ha-Ras, and pCMV LacZ (17, 18) are used in the study.

Compound library screen. The cell-based assays used dual reporter gene read-outs. The test HCT116 reporter clone (Ras-Net) expresses Gal4-Net (220–409), Gal4 UAS–Renilla luciferase, and Ras Val12 (to enhance reporter gene expression). The control SW480 cell clone expresses β-catenin that activates firefly luciferase expression from a Tcf/Lef-dependent promoter. The cells in 384-well plates were treated with compounds (500,000) for 24 h before measuring the luciferases.

Transient transfections. NIH3T3 cells were transfected using the calcium phosphate technique; luciferase and control β-galactosidase activities were assayed. Fold activation relative to control vectors was determined in three experiments with two plasmid preparations.

Treatment with compounds and fibroblast growth factor 2. Cells were grown overnight from 80% to 90% confluence, incubated in 0.05% (NIH3T3) or 0.1% (human umbilical vascular endothelial cell, HUVEC) serum for 4 h, treated with compounds for 3 h (NIH3T3) or 1.5 h (HUVEC), 20 ng/mL fibroblast growth factor 2 (FGF-2) for 1 to 90 min, and lysed in Laemmli buffer containing phosphatase and protease inhibitors.

Quantitative real-time reverse transcription–PCR. Total RNA was used. Primers were designed with Oligo 4.0. Amplification specificity was verified by melting curve analysis, and the data were quantified with LightCycler software. The controls for genomic DNA contamination were not reverse transcribed.

Western blotting and antibodies. Cells were harvested in Laemmli buffer, fractionated by 10% SDS-PAGE, transferred to nitrocellulose membranes, incubated with primary antibodies, horseradish peroxidase–conjugated secondary antibodies, and revealed with SuperSignal Pico West (Pierce).

Ras activation assay. The Ras activation assay kit (Cytoskeleton, BK008) was used. The controls for loading and signaling pathway activation used cell lysates before affinity chromatography and Western blotting for glyceraldehyde-3-phosphate dehydrogenase (GAPDH) and phosphorylated Erk-1/2, respectively.

Fluorescence-activated cell sorting. Cells were grown, synchronized in low serum (0.1% for NIH3T3) overnight, treated with compounds for 20 h in medium with serum (10% FCS for NIH3T3), and analyzed by fluorescence-activated cell sorting (FACS) (19) and the CellQuest program (Becton Dickinson). The experiments were repeated at least thrice with 5 to 500 nmol/L XRP44X.

Mouse aortic ring angiogenesis assay. Thoracic aortas sections (1-mm long) from 8-week-old 129/PAS mice were placed in Matrigel, incubated for 48 h in EGM-2-MV (CC-3202, Clonetics), followed by 3 days in fresh EBM-2-MV containing various compounds. Microvessel sprouts were examined by biomicroscopy and a Cool SNAP camera. The experiments were repeated thrice.

Cell proliferation. Cells (2×10^3 per well) were seeded in 96-well plates allowed to attach for 12 h. Growth curves were from 10 nmol/L compounds for samples every 24 h. For IC_{50} values, at logarithmically increasing amounts of compounds, samples were analyzed after 2 (HCT-116 and NIH3T3–Ki-Ras) or 3 days (HUVEC and NIH3T3). The WTS-8 cell counting kit was used (Alexis Biochemical). The experiments were repeated thrice, with six wells per condition in each experiment. IC_{50} values were determined by curve fitting (MatLab) and semilogarithmic plotting.

Immunocytochemistry. Cells on coverslips were treated with compounds, fixed with acetone/methanol (1:1), and revealed with phosphorylated Net (P-Net) or β-tubulin monoclonal antibodies followed by FITC-conjugated antimouse antibodies. For actin, the cells were fixed with 3.7% formaldehyde, permeabilized with 0.1% Triton X-100, and treated with Texas red–conjugated phalloidin. Nuclei were stained with 4′,6-diamidino-2-phenylindole (DAPI; Sigma).

Results

A high throughput cell-based screen for inhibitors of Ras-induced transcription activation. To identify small molecules that inhibit Ras oncogene–induced Net transcription activation, a HCT116 reporter cell line was established (HCT116-Net-Ras). It expresses two proteins, oncogenic Ha-Ras and the Net-Ras responsive transcription activation domain (215–409) fused to the Gal4 DNA-binding domain (Gal4-N5; Fig. 1*A*), and in addition, it contains a Gal4 UAS-Renilla luciferase reporter. A counter-screening SW480 cell line was produced containing the Firefly luciferase gene under the control of a β-catenin/T-cell factor promoter sequence (data not shown). A library of small molecules was screened, resulting in the identification of XRP44X, a 3-piperazinylcarbonyl-pyrazole (Fig. 1*B*) that inhibited Ras-induced transcription activation (IC_{50}, 10 ± 6.5 nmol/L; Supplementary Table S1) with little effect on the β-catenin/T-cell factor–dependent transcription activation (IC_{50}, >3,000 nmol/L). The properties of XRP44X were studied in comparison with its regioisomer XRP45X and with the related molecule XRP57X and its regioisomer XRP58X.

The effects of these compounds on Net activity were investigated using the HCT116-Net-Ras reporter cell line (Supplementary Table S1). XRP44X inhibited luciferase activity more efficiently than its regioisomer XRP45X (IC_{50}, ~10 and 700 nmol/L, respectively), the related molecule XRP57X (IC_{50}, ~80 nmol/L), and its regioisomer

XRP58X (IC_{50}, ~1,500 nmol/L). These values were determined from dose-response curves and reflect true differences rather than "plateau effects." The effects were not merely due to general cytotoxicity, because there was no significant variation in the total protein concentration extracted from the cultures and the compounds had no effect on the β-catenin/T-cell factor–responsive cell line. To test the effect of XRP44X on the activity of full-length Net, transfection experiments in NIH3T3 fibroblasts were used. A Ras-responsive reporter (Palx8-TK-Luc; ref. 17) was cotransfected with expression vectors for Net, Ha-Ras-Val12 to activate Net, and β-galactosidase as an internal control. XRP44X inhibited Net activity to a greater extent than the other compounds (Supplementary Table S1). The Erk-1/2 pathway inhibitor U0126, which inhibits Net phosphorylation and activation (10), also decreased luciferase activity. General toxicity could not account for the effects of the compounds because there was no significant variation in β-galactosidase activity. These results indicate that XRP44X inhibits Ras-induced activation of Net efficiently and specifically.

XRP44X inhibits Net phosphorylation. Growth factors stimulate the Ras-Erk-TCF pathway rapidly and transiently, leading to changes in gene expression (20). We investigated the effect of XRP44X on FGF-2 induction of the endogenous *c-fos* and *egr-1* genes by quantitative real-time reverse transcription–PCR. Mouse fibroblasts (NIH3T3 cells) were pretreated for 3 h with 100 nmol/L XRP44X, treated with FGF-2 for 40 min, and analyzed for *c-fos* and *egr-1* RNA expression. XRP44X inhibited expression of both genes by ~65% (Supplementary Table S2). HUVECs were studied more extensively (Supplementary Fig. S1) to determine the effects on the time course (A and B) and the dose dependency (C and D). Fifty percent inhibition of *egr-1* and 65% of *c-fos* were observed with 200 nmol/L XRP44X 60 min after FGF-2 induction (C and D). The extent of inhibition was similar after 30 min (A and B). There were no significant variations in 28S RNA levels, showing that the decrease was not due to nonspecific effects. Taken together, these results indicate that the 3-piperazinylcarbonyl-pyrazole XRP44X inhibits transcription activation induced by the growth factor–Ras-Net pathway.

Because *c-fos* and *egr-1* are Net target genes and Net is activated by Erk phosphorylation, we investigated whether inhibition resulted from effects on Net phosphorylation. Growth factors stimulate phosphorylation of the COOH terminal domain of Net through the Ras-Erk pathway. Phosphorylation of Ser^{363}, which is one of the most important phosphorylation sites for activation of the COOH terminal domain, was followed using the MAb2F3 phosphorylated-specific antibody (10, 21). Normal HUVEC were serum starved for 24 h and treated with 20 ng/mL FGF-2 and Net phosphorylation, followed by Western blotting with the phosphorylated-specific antibody (Fig. 2*A*). Net phosphorylation was detected after 5 min (*lane 4*), was maximal after 10 min (*lane 5*), and gradually declined up to 45 min (*lane 8*). There was a shift in mobility of Net that could be correlated with the intensity of the bands, as might be expected from the phosphorylation of several sites on Net (10, 21). Changes in intensity of the bands were reproducibly observed in HUVEC and other cell lines (NIH3T3 mouse fibroblasts, C6 rat glioma, LL/2 mouse Lewis lung carcinoma, SEND skin endothelial cells transformed with polyoma middle T and HCT116 colon carcinoma cells, but not NIH3T3–Ki-Ras and PC3 prostate carcinoma cells; Supplementary Fig. S2 and data not shown), whereas the shift was more variable and depended on the cell line used, the particular conditions of electrophoresis and the initial state of phosphorylation of Net (Supplementary Fig. S2*A* and data not shown). Similar to Net, the related protein Elk-1 has been extensively characterized and shown to have several phosphorylation sites of varying importance for transcription activation (22). In some experiments, the 2F3 phosphorylated-specific antibody detects additional nonidentified bands in HUVEC cells (Fig. 2; see also Supplementary Fig. S2*A* and *B*). The identities of these bands are not known and could correspond to other modified forms of Net or other proteins. They do not compromise the identification of the P-Net bands nor the interpretations of the experiments, which have been repeated a large number of times in HUVEC and in a number of other cell lines.

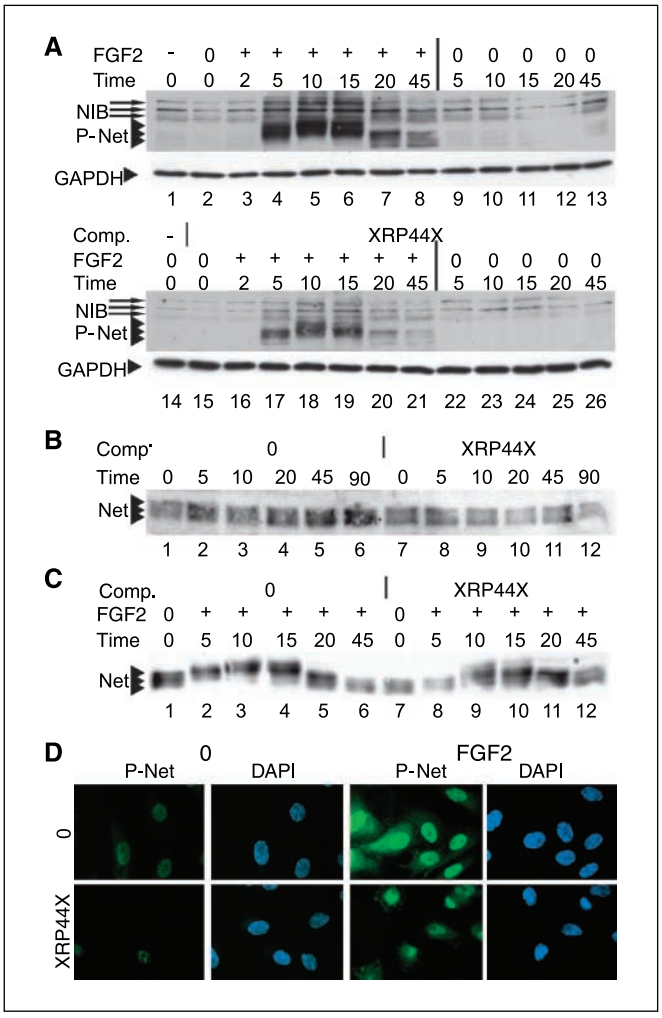

Figure 2. XRP44X inhibits FGF-2–induced Net phosphorylation (serine 363) in HUVEC. *A,* kinetics of Net phosphorylation induced by FGF-2. HUVEC cells were incubated for 4 h in low serum (0.1% FCS), pretreated with XRP44X (100 nmol/L) or vehicle (DMSO) for 90 min, and then induced with FGF-2 (20 ng/mL) for 0 to 45 min. Conditions: FGF-2 for 0 to 45 min (*lanes 2–8 and 15–21*), mock-induced with vehicles (*lanes 9–13 and 22–26*), noninduced (*lanes 1* and *14*; samples taken at the end of the experiment), pretreated with XRP44X (100 nmol/L; *lanes 15–26*), and mock pretreated (*lanes 2–13*). Cell extracts were analyzed by Western blotting for P-Net (MAb2F3) and GAPDH. *B* and *C,* changes in overall Net protein expression do not account for differences in P-Net levels. Conditions were as in *A*, except that PAb2005 was used for Western blotting. *D,* XRP44X inhibits FGF-2–induced Net phosphorylation in the nucleus. HUVEC were incubated in low serum for 4 h, pretreated with vehicle (0; *top*) or XRP44X (100 nmol/L; *bottom*) for 90 min, treated with FGF-2 for 10 min, and processed for immunocytochemistry using MAb2F3. DAPI stains nuclei. Typical representative fields.

To investigate whether the compound inhibited Net phosphorylation, HUVEC cells were pretreated with 100 nmol/L XRP44X for 90 min and then treated with FGF-2. XRP44X clearly inhibited Net phosphorylation by ~80%, without affecting the kinetics of the residual phosphorylation that could still be detected (Fig. 2*A, lanes 17–21*). XRP44X treatment alone did not induce Net phosphorylation (*lanes 22–26*). The total levels of Net, detected with an antibody raised against the COOH terminal region of Net (polyclonal antibody 2005), did not significantly change during the course of the experiment (Fig. 2*B, lanes 1–12*; data not shown). There was a shift in the mobility (Fig. 2*C, lanes 1–12*) that coincided with the shift observed with the phosphorylated-specific antibody and probably reflects the effect of phosphorylation on migration once FGF-2 is added to the cells. The levels of the loading control GAPDH remained constant (Fig. 2*A, lanes 1–26*). Inhibition of Net phosphorylation was observed with a range of concentrations of XRP44X (20 nmol/L–5 μmol/L; data not shown). XRP44X was also found to inhibit Net phosphorylation in other cell lines, including NIH3T3 fibroblasts, C6 glioma cells, LL/2, and SEND (Supplementary Fig. S2). In NIH3T3 cells, preincubation in the absence or presence of XRP44X for up to 180 min did not affect the levels of Net protein (polyclonal antibody 375; Supplementary Fig. S2*C, lanes 1–12*). Similarly, preincubation with the Mek inhibitor U0126 inhibited Net phosphorylation without affecting total Net protein (Supplementary Fig. S2*D, lanes 1–4*). XRP45X, XRP57X, and XRP58X were considerably less efficient than XRP44X in inhibition of Net phosphorylation induced by FGF-2 (Supplementary Fig. S2*B, lanes 5–10*). These results show that XRP44X inhibits Net prosphorylation without altering total protein levels.

Net phosphorylation was also evaluated by immunocytochemistry of HUVEC with MAb2F3 (Fig. 2*D*). FGF-2 treatment for 10 min led to a clearly detectable increase in P-Net in cell nuclei. This staining was more intense than in cells pretreated for 90 min with XRP44X. The remaining detectable P-Net in XRP44X-treated cells was still mainly located in the nucleus. Similar results were obtained in NIH3T3 cells (Supplementary Fig. S3). The results from Western blotting and immunocytochemistry show that XRP44X inhibits Net phosphorylation on Ser^{363} in the nuclei of cells.

XRP44X inhibits FGF-2 activation of the Erk-1/2 pathway. We have previously shown that FGF-2 stimulates Net phosphorylation through the Erk-1/2 pathway (10), raising the possibility that XRP44X inhibits this signaling cascade. Erk-1/2 activation involves formation of Ras-GTP, Raf recruitment, sequential phosphorylation, activation of Raf-1, Mek-1/2, and Erk-1/2, and finally phosphorylation by Erk-1/2 substrates, such as Rsk (23), as well as Net. We tested whether XRP44X affects this cascade. XRP44X inhibited phosphorylation of Rsk-1 (Fig. 3*A*), showing that XRP44X is not a specific inhibitor of Net phosphorylation. XRP44X inhibited phosphorylation of Erk-1/2 on sites required for its activation without affecting overall levels of Erk-1/2 (Fig. 3*A*). Furthermore, it inhibited phosphorylation of Mek-1/2 and Raf-1 (Fig. 3*A*) and activation of Ras (Fig. 3*B*; see also Fig. 6*C*). Because the observation that XRP44X inhibits Ras activation is important, we also measured Ras activation with an ELISA-based assay. In time course experiments, maximum Ras activation was observed after 5 min (Supplementary Fig. S4), in agreement with the pull-down assays (Fig. 3*B*). In dose-response experiments, maximum inhibition was observed with 100 nmol/L XRP44X. These results show that XRP44X is an indirect inhibitor of Net phosphorylation that acts upstream from Erk-1/2 activation. This is not necessarily unexpected, considering that a cell-based screen and a functional readout were used to isolate XRP44X.

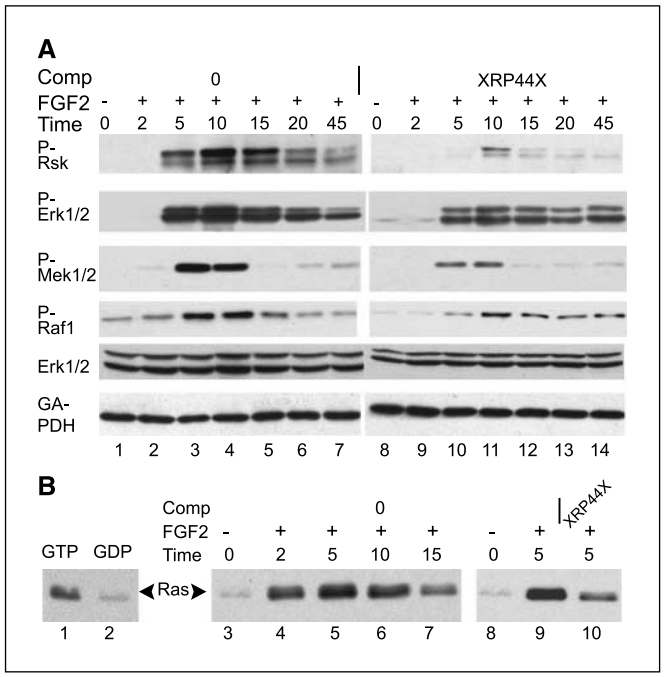

Figure 3. XRP44X inhibits activation of the Ras–Erk-1/2 pathway by FGF-2. *A,* activation of the Raf-1–Erk-1/2 cascade. HUVEC cells were incubated for 4 h in low serum (0.1% FCS), pretreated with XRP44X (100 nmol/L) or vehicle (DMSO) for 90 min, and then induced with FGF-2 (20 ng/mL) for 0 to 45 min. Extracts were analyzed by Western blotting for phosphorylation of p90Rsk (*P-Rsk*; Thr^{359}/Ser^{363}), Erk-1/2 (*P-Erk-1/2*, Thr^{202}/Tyr^{204}), Mek1/2 (*P-Mek1/2*, $Ser^{217/221}$), Raf-1 (*P-Raf1*, Ser^{338}). Total Erk-1/2 and GAPDH were controls. *B,* Ras activation. To estimate the potential range of conversion of inactive Ras-GDP to active Ras-GTP, extracts from HUVEC growing in complete medium with FCS were loaded with excess GTP-γ-S (*lane 1*) and GDP (*lane 2*), and proteins "pulled down" with Raf-RBD beads were analyzed by Western blotting for Ras. To measure the kinetics of Ras activation by FGF-2, HUVEC cells were incubated for 16 h in low serum (0.1% FCS) and induced with FGF-2 (20 ng/mL) for 0 to 15 min (*lanes 3–7*). To study the effects of XRP44X on Ras activation, HUVEC cells were incubated for 16 h in low serum (0.1% FCS), preincubated with XRP44X or vehicle for 90 min, and induced with FGF-2 (20 ng/mL) for 5 min (*lanes 8–10*).

XRP44X inhibits microvessel sprouting from aorta in organ cultures and cell growth. The mechanisms by which XRP44X inhibits the Ras-Erk pathway was investigated further using a variety of assays that led to insights into its activities. One of these approaches was to study cellular processes that are regulated by Net, including microvessel sprouting from aorta in organ culture and cell growth (10). In the aorta ring assay (Fig. 4*A*), XRP44X inhibited microvessel sprouting when the aorta were incubated with 5 nmol/L XRP44X for 3 days (compare panels 1 and 3). The inhibition was greater when 50 nmol/L XRP44X was used (panel 5). To study regrowth after removal of the inhibitor, XRP44X was soaked out of the semisolid medium by washing and adding fresh medium lacking XRP44X to the 50 nmol/L XRP44X cultures. Microvessel sprouting was clearly restimulated (panel 8), showing that regrowth was possible when the concentration of XRP44X was decreased. Inhibition of aortic sprouting by XRP44X was observed in three different experiments with three aorta cultures per treatment and 5, 10, 20, and 50 nmol/L XRP44X (data not shown). As a positive control, the mitogen-activated protein/ERK kinase 1/2 inhibitor U0126 was shown to inhibit microvessel sprouting (panels 2 and 4), and

washing out the inhibitor restored growth (compare panel 7 with panel 6), as expected from the known role of Erk-1/2 signaling in aortic sprouting (24).

The effect of XRP44X on the growth of endothelial cells (HUVEC) was followed with a modified 3-(4,5-dimethylthiazol-2-yl)-2,5-diphenyltetrazolium bromide assay (WTS-8). XRP44X inhibited their growth (Fig. 4*B*), with an IC_{50} of ~2 nmol/L (Supplementary Table S3). XRP44X also inhibited the growth of immortalized mouse fibroblasts (Fig. 4*C*), the human tumor cell line used to develop the HTS target cell line (HCT-116; Fig. 4*D*), and the Ki-Ras transformed cell line derived from the NIH3T3 cell line clone shown (Fig. 4*E*). The IC_{50} values for the endothelial cells, the human tumor cell line, and the transformed fibroblast line were similar. The nontransformed fibroblasts used for Ki-Ras transformation had a slightly higher IC_{50} (Supplementary Table S3), indicating that Ki-Ras transformation might increase the sensitivity to XRP44X. The antiproliferative activity of XRP44X relative to the related compounds (XRP45X, XRP57X, and XRP58X) was measured

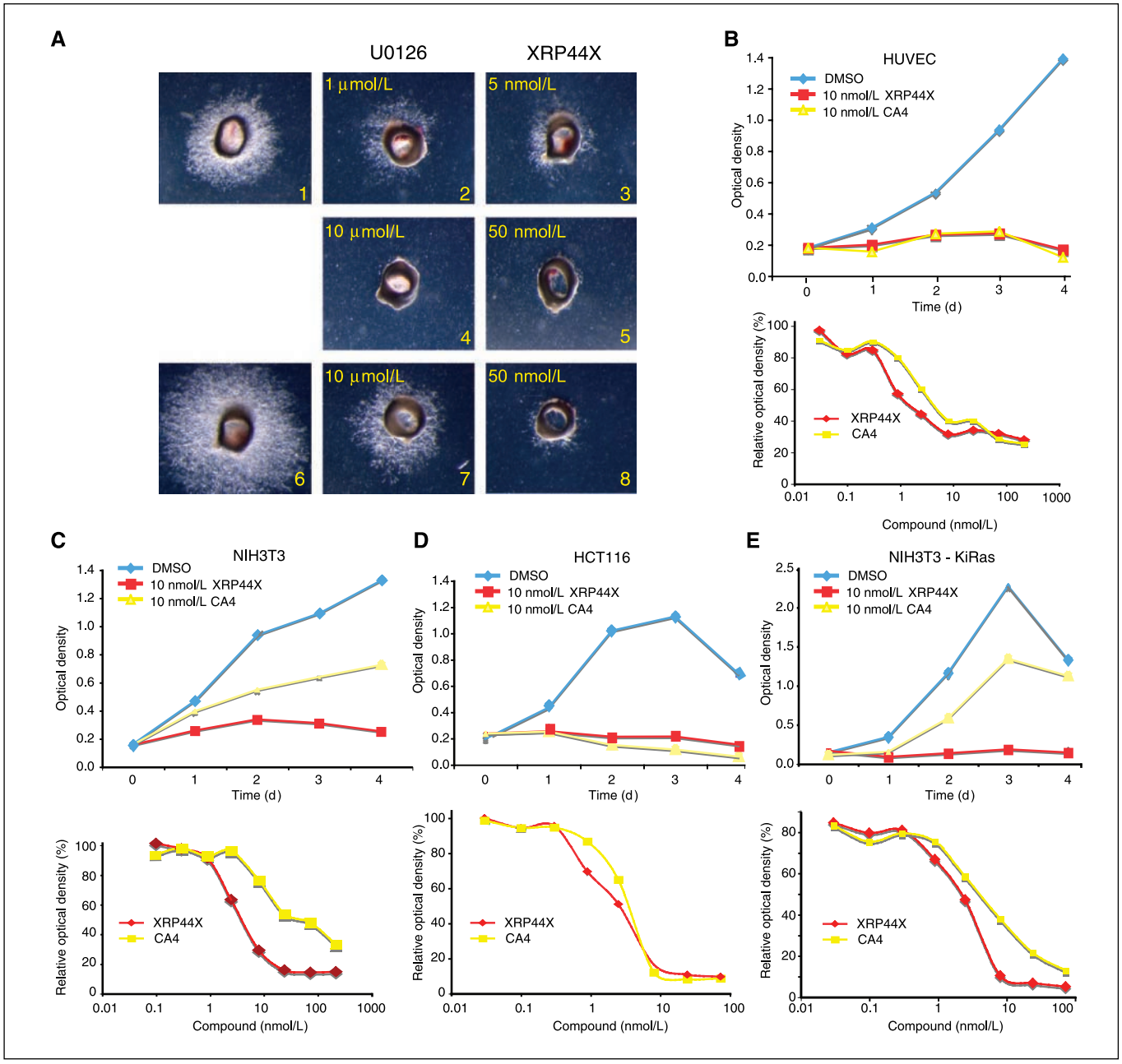

Figure 4. Inhibition by XRP44X of aortic microvessel sprouting (*A*), and inhibition by XRP44X and CA4 of proliferation of cells (*B–E*) as a function of time (*top graphs*) and concentration (*bottom graphs*). *A,* aorta were implanted in 300 µL Matrigel, overlaid with 1 mL complete medium containing growth factors and serum and incubated for 2 d. The medium was replaced with fresh medium containing vehicle (*panels 1* and *6*), U0126 (*panels 2, 4,* and *7*), or XRP44X (*panels 3, 5,* and *8*), as indicated. After 4 d, the cultures were photographed (*panels 1–5*), washed thrice, incubated for a further 2 d without compounds, and photographed (*panels 6–8*). *B–E,* cells were seeded in 96-well plates (2×10^3 per well), allowed to attach, and, after 12 h, treated with 10 nmol/L of XRPX44X or CA4, and proliferation was measured with the WTS-8 assay every 24 h for 4 d (*top graphs*). The effects of different concentrations of the compounds on proliferation were measured after 3 d for HUVEC and NIH3T3 (*B, C*) and 2 d for HCT-116 and NIH3T3–Ki-Ras (*D, E*).

with a thymidine incorporation assay on various cell lines derived from the most common human tumors. XRP44X inhibited proliferation more efficiently than its regioisomer XRP45X, and the related molecule XRP57X and its regioisomer XRP58X (Supplementary Table S4). These results show that XRP44X specifically inhibits growth of cells derived from many common human tumors.

XRP44X leads to G_2-M cell cycle arrest and alters the tubulin and actin cytoskeletons. The mechanisms by which XRP44X affects cell growth were examined further using cell cycle analysis, visual inspection, and immunocytochemistry in various cell types, especially NIH3T3 fibroblasts and HUVEC endothelial cells. For FACS analysis, NIH3T3 cells were synchronized by incubation overnight in medium containing 0.1% FCS. They were then incubated in high serum (10% FCS) in the presence of vehicle (control), 50 nmol/L XRP44X, or XRP45X. The treatment with XRP44X resulted in the accumulation of cells in the G_2-M phase in comparison with XRP45X or control (Fig. 5*A*), which is compatible with the observed inhibition of cell growth (see above; similar results were obtained with HUVEC and several other cell lines; data not shown). Cells were visually inspected by phase contrast microscopy. HUVEC were incubated in the conditions used to analyze signal transduction (see above), namely 4 h in low serum followed by 90 min with 50 nmol/L XRP44X or XRP45X, fixed, and observed under the microscope (Fig. 5*B*, visible). XRP44X was found to induce "blebbing" of the cell surface in contrast to XRP45X (data not shown) or vehicle control. Similar effects were observed with NIH3T3 and other cell lines (data not shown). These changes are reminiscent of CA4, which has effects on both tubulin microtubules and the actin cytoskeleton (25–27). Immunocytochemistry was used to examine microtubules using antibodies against β-tubulin. Treatment of HUVEC cells with XRP44X led to disorganization of the tubulin microtubules in contrast to XRP45X (data not shown) and the control (Fig. 5*B*). This effect of XRP44X is similar to the effects already described for CA4 (25–27) and reproduced in Fig. 5*B*. We then compared the effects of XRP44X and CA4 on Filamentous actin (F-actin) using rhodamine-phalloidine (Fig. 5*C*). Both compounds had similar effects on the actin cytoskeleton, leading to the formation of actin-lined cell surface protrusions (blebs). Similar effects on the actin cytoskeleton were observed in NIH3T3 (data not shown). Using FACS analysis, we also confirmed that CA4 blocked cells in the G_2-M phase, similar to XRP44X (data not shown). CA4 binds to the colchicine site and depolymerizes microtubules (27). We showed that XRP44X binds to the same site as CA4 on tubulin and also depolymerizes microtubules (Supplementary Table S5). We also showed that CA4 inhibits proliferation of HUVEC, NIH3T3, HCT-116, and NIH3T3–Ki-Ras (Fig. 4*B–E*), with IC_{50} values similar to XRP44X (Supplementary Table S3). These results show that XRP44X and CA4 have similar effects on cells and may act by similar mechanisms.

CA4 efficiently inhibits Net phosphorylation and activation of the Erk pathway by FGF-2 in contrast to docetaxel, vincristine, or nocodazole. Tubulin-interacting molecules bind to different sites and have different effects on microtubules (28). We compared the effects of XRP44X with CA4 that binds to the same site of tubulin, as well as with docetaxel that interacts with the taxane site and stabilizes microtubules and vincristine that interacts with the Vinca site and blocks tubulin assembly. HUVEC cells were treated for 90 min with increasing amounts

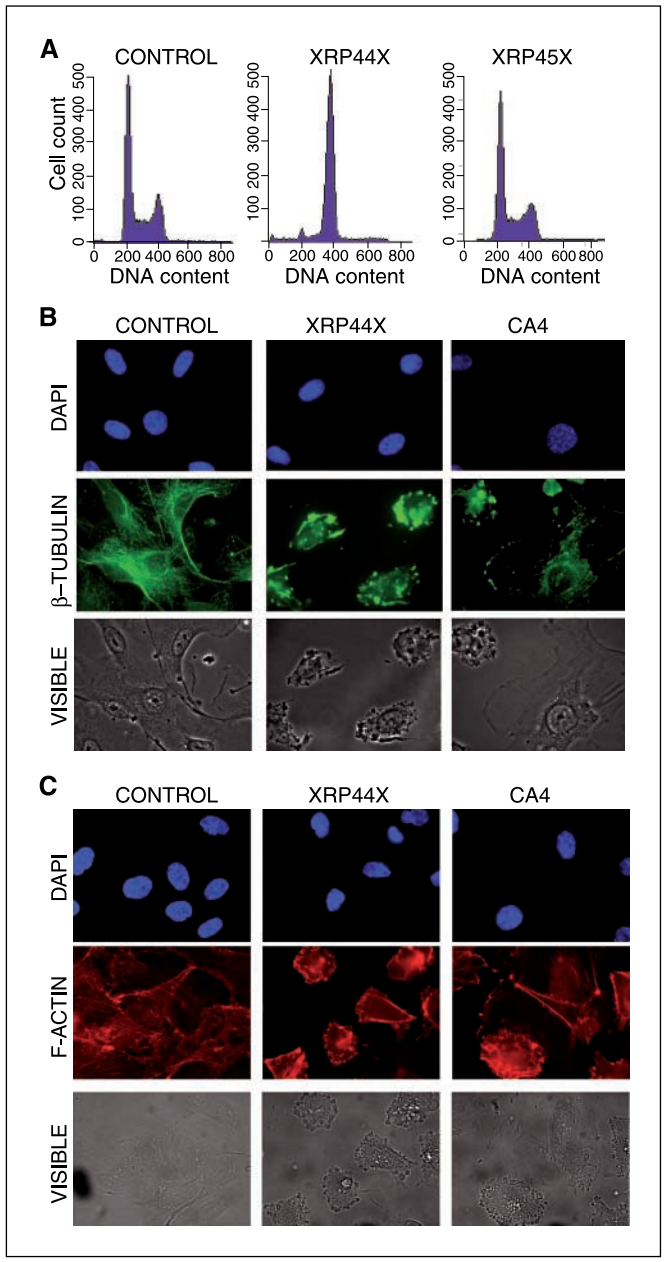

Figure 5. XRP44X treatment leads to accumulation of cells in the G_2-M phase of the cell cycle and disorganization of the tubulin and actin cytoskeletons. *A,* NIH3T3 cells were incubated overnight in low serum (0.1% FCS) followed by 24 h in high serum (10% FCS) in the presence of vehicle (control), 50 nmol/L XRP44X, or XRP45X and analyzed by FACS. Similar effects were observed with a range of concentrations of XRP44X (5–500 nmol/L). One representative experiment is shown. *B* and *C,* HUVEC cells were incubated for 4 h in 0.1% FCS, 90 min with 50 nmol/L XRP44X, 50 nmol/L CA4, or vehicle alone (control) and processed for immunocytochemistry with antibodies against β-tubulin and FITC secondary antibodies, rhodamine-phalloidine to stain F-actin, and DAPI for nuclei. Cells were observed under visible light and by fluorescence microscopy. Representative fields are shown.

of the compounds, and Net phosphorylation induced by FGF-2 was examined by Western blotting (Fig. 6*A*). CA4 inhibited Net phosphorylation at similar concentrations as XRP44X (IC_{50}, ~20 nmol/L; Fig. 6*A, lanes 1–12*). In contrast, docetaxel did not affect Net phosphorylation, even when the concentration was increased to much higher levels than XRP44X or CA4 (*lanes 13–18*). Vincristine also had little effect on Net phosphorylation

(*lanes 19–24*; IC_{50}, ≥1 μmol/L). We tested nocodazole that also binds to the colchicine site. We found that nocodazole was significantly less efficient than XRP44X in inhibiting Net phosphorylation (*lanes 25–30*). The compounds did not affect the amounts of the internal control (GAPDH; data not shown). Similar results were obtained in NIH3T3 cells (Supplementary Table S6 and Supplementary Fig. S5).

We also tested whether CA4 affects the Erk signaling cascade (Fig. 6*B* and *C*). CA4 inhibited FGF-2–induced expression of *egr-1* and *c-fos* (Supplementary Fig. S1*A* and *B*) to a similar extent as XRP44X and with a similar dose response (Supplementary Fig. S1*E* and *F*). CA4 also inhibited phosphorylation of Rsk, Erk-1/2, Mek-1, and Raf-1 (Fig. 6*B, lanes 1–13*; the inhibition of Raf-1 by XRP44X and CA4 was confirmed by quantification of scans and correction for the internal control GAPDH; data not shown). CA4 also inhibited activation of Ras (Fig. 6*C*). We confirmed the inhibition of Ras activation using an ELISA assay (Supplementary Fig. S4). In contrast, docetaxel did not inhibit, but rather had a small positive effect on Erk-1/2 activation that was observed in this and some other experiments (Fig. 6*B, lanes 14–20*; data not shown). Similarly, nocodazole had no prominent effect on the Erk signaling cascade under these conditions (*lanes 21–26*; data not shown). In line with the positive effect of docetaxel on Erk-1/2, it was found to increase FGF-2 induction of the endogenous *c-fos* and *egr-1* genes (Supplementary Table S2). Docetaxel and U0126 (that inhibits Mek-1) did not affect Ras activation (Fig. 6*C*; data not shown). These results provide evidence that XRP44X and CA4 have similar mechanisms, which are not common to other classes of tubulin binders and even to nocodazole that belongs to colchicine site binder class.

Discussion

We have identified an inhibitor of Ras-induced transcription activation through the MAPK pathway. It inhibits growth factor–induced gene expression through the Erk signaling pathway, alters the morphology of microtubules and the actin cytoskeleton, affects transcription regulation, and blocks cell cycle progression and microvessel sprouting. Different mechanisms may contribute to the effects observed in these short, medium,

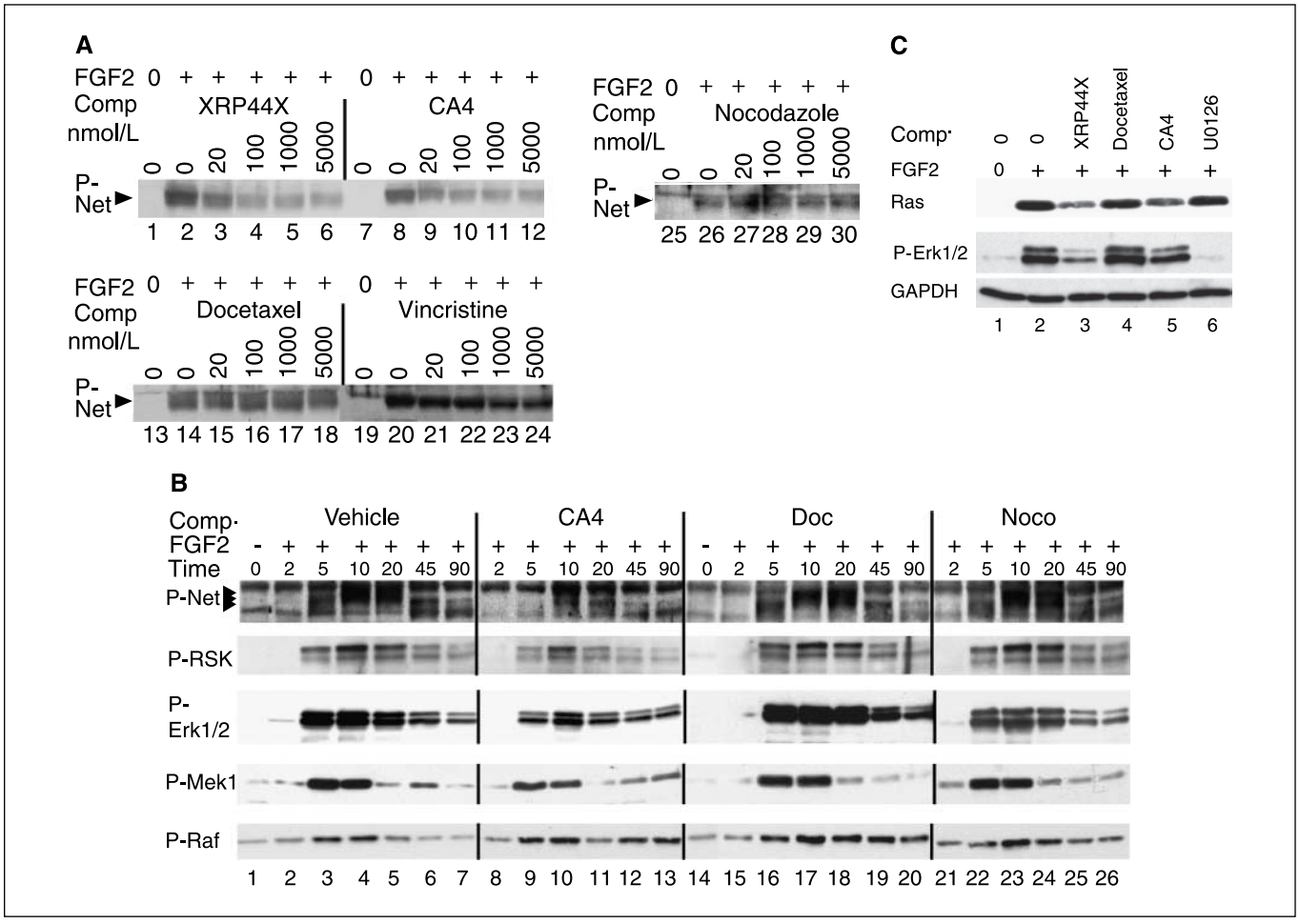

Figure 6. Inhibition of Net phosphorylation and the Ras–Erk-1/2 pathway by microtubule inhibitors. *A,* XRP44X and CA4 inhibit Net phosphorylation, in contrast to docetaxel, vincristine, and nocodazole. HUVEC cells were incubated for 4 h in 0.1% FCS, 90 min with the indicated compounds, and 10 min with 20 ng/mL FGF-2 and analyzed by Western blotting with MAb2F3 to detect P-Net. *B,* inhibition of Erk-1/2 pathway activation. HUVEC cells were incubated for 4 h in 0.1% FCS, 90 min with 100 nmol/L CA4, docetaxel, or nocodazole, and 0 to 90 min with 20 ng/mL FGF-2. Cell extracts were analyzed by Western blotting with phosphorylated-specific antibodies. *C,* inhibition of Ras activation. HUVEC cells were incubated for 16 h in low serum (0.1% FCS), 90 min with 100 nmol/L XRP44X, docetaxel, CA4, or U0126, and induced with FGF-2 (20 ng/mL) for 5 min. Cell extracts were used directly for Western blotting to detect phosphorylated Erk-1/2 and GAPDH (loading control). The activation state of Ras was determined by "pull down" with RBD beads and Western blotting with a pan-Ras antibody.

and long-term assays. One of the interesting properties is that it is a microtubule poison, a class of molecules already successfully used in cancer treatment. Microtubule poisons have different effects and fall into distinct classes based on their effects on tubulin and microtubule dynamics and also on "additional" effects that are increasingly being investigated. Understanding these, "secondary" pathways are important for the design and optimum use of cancer therapeutics.

The inhibitor XRP44X was identified in a cell-based screen for decreased luciferase activity driven by Ras-induced activation of Net. XRP44X is an efficient inhibitor of Ras-Erk–mediated phosphorylation of Net (IC_{50}, 10–20 nmol/L). Compound inhibitory activity is structurally specific because the regioisomer XRP45X and close analogues (XRP57X and XRP58X) are much less efficient. The screen was focused on the Ras-Net pathway, with a counter selection for compounds that affected the β-catenin/T-cell factor pathway. In short-term transfections, XRP44X inhibited Ras-induced activation of both the fusion proteins used in the original screen (Gal4-N5; data not shown), as well as full-length Net with a different reporter, without having an effect on the internal control. XRP44X also inhibited the expression of several endogenous genes that are induced by the Ras-Erk pathway, *c-fos* and *egr-1*. These results indicate that XRP44X is relatively selective and specific in its effects.

We investigated the mechanisms by which XRP44X affects the Ras-Net pathway. The COOH terminal domain of Net used in the screen is activated by Erk phosphorylation on Ser^{363}, which can be followed with a phosphorylated-specific antibody (21). Treatment of different cell types with XRP44X inhibited phosphorylation of endogenous Net on Ser^{363}. We traced the origins of the inhibition by working backwards along the pathway. Net is regulated by nuclear export in response to several stress-induced pathways (29). Net remained in the nucleus under the conditions used (see Fig. 2; Supplementary Fig. S3 and data not shown), indicating that XRP44X did not significantly induce export of Net but rather suggesting that it inhibited Erk-1/2 activity. Erks are activated by phosphorylation in the cytoplasm, and they, in turn, phosphorylate cytoplasmic proteins and nuclear proteins after migration into the nucleus (30). Inhibition of nuclear import of Erk-1/2 could have led to decreased phosphorylation of Net, which is found in the nucleus. However, we did not observe effects on nuclear import (data not shown) in agreement with other studies (review ref. 31). We showed that phosphorylation of Erk was inhibited and that the remaining detectable activated Erk-1/2 was found in both the cytoplasm and nucleus, using immunocytochemistry and subcellular fractionation (see above and data not shown). These results indicated that the major effect of XRP44X was upstream from Erk-1/2. We traced the inhibition upstream through Mek1/2, Raf-1, and Ras-GTP, showing that XRP44X inhibits Ras activation. This inhibition could come from effects of XRP44X on the cytoskeleton. Cell staining for actin and tubulin showed alterations in cytoskeletal architecture. XRP44X stimulates microtubule depolymerization *in vitro* and competes with colchicine for binding to tubulin. CA4 has similar effects on the cytoskeleton and microtubules (27, 32, 33), inhibits the Ras-Net signaling pathway (this study), and induces early membrane blebbing through a mechanism that involves activated Erks (25), suggesting that they act by similar mechanisms. Interestingly, nocodazole, which also belongs to colchicine "binder" class of compounds, does not inhibit the Ras-Net signaling pathway, demonstrating that microtubule depolymerization can be uncoupled from inhibition of this pathway.

Despite ~20 years of research since the original isolation and synthesis of CA4 (34), the precise mechanisms by which it operates are incompletely understood. Importantly, CA4 has been shown to rapidly activate the small GTPase Rho and Rho-kinase (25). In line with this, we have found that XRP44X affects ezrin expression and phosphorylation, using macroarrays and phosphorylated-specific antibodies (data not shown). Ezrin belongs to the ezrin/radixin/moesin (ERM) family of actin binding proteins that act as signal transducers in response to cytoskeleton remodeling. ERM proteins are linked to Rho signaling through several pathways (35). Further studies focused on already described endogenous inhibitors of the Ras-Erk pathway (review ref. 36) may help to unravel the molecular mechanism by which CA4 and XRP44X selectively affect cellular signaling.

As expected for a microtubule poison, XRP44X in cell culture inhibits cell proliferation and leads to the accumulation of cells in the G_2-M phase without obvious cell type specificity. XRP44X inhibits sprouting from aorta in *ex vivo* experiments (see above). XRP44X behaves as a typical tubulin poison that binds to the colchicine-binding site. The effects of XRP44X are very similar to those described for combretastatins (review ref. 27), suggesting by analogy that XRP44X is potentially a vascular-disrupting agent. Interestingly, we have shown that Net is expressed at sites of angiogenesis and tumorigenesis during development and has a role in angiogenesis in *in vitro, ex vivo*, and *in vivo* assays (8–10), suggesting that targeting Net in the screen for XRP44X favored selection of a vascular-disrupting agent. However, XRP44X, like combretastatins, is not specific for endothelial cells, and the relative importance of its effects on different cell types (endothelial cells, tumor cells) in inhibition of tumor growth and metastasis remains to be established.

Many microtubule-targeted drugs have been described, and microtubules are good targets for anticancer therapy (review refs. 13, 14). The drugs bind to different sites on tubulin, in particular the taxane, *Vinca*, and colchicine domains. Taxanes stabilize microtubules, whereas *Vinca* alkaloids, nocodazole, combretastatins, and XRP44X destabilize microtubules (Supplementary Table S6). Differences in their effects on microtubules are probably reflected in the biological properties of the drugs. We found that docetaxel did not inhibit Ras-Net signaling, and vincristine was much less efficient (IC_{50}, ~1 μmol/L). Our results agree with other studies that show that paclitaxel does not inhibit MAPK activation (37, 38). Furthermore, we found that docetaxel has a slight positive effect on c-fos expression in contrast to XRP44X. Similar effects on c-fos expression and associated activation of Erk-1/2 have been described recently (39, 40). Taxoids and microtubule-destabilizing agents have opposite effects on *c-myc* oncogene expression in some cell types (41) through mechanisms involving nuclear factor-κB (NF-κB; ref. 42). They have been reported to use the NF-κB pathway to stabilize HIF-1α, a factor that is important for wound healing and angiogenesis by regulation of cell response to hypoxia (43). Interestingly, Net is also implicated in wound healing, angiogenesis, and the response to hypoxia (refs. 8–10; data not shown), indicating that MDAs may regulate several different pathways that are important in common physiologic processes. Knowledge of the differences in transcription factor control by microtubule-targeted drugs may be used to increase their therapeutic potential. Fascinatingly, the therapeutic efficacy of Paclitaxel can be enhanced by inhibition

of the Erk activator Mek in nude mice bearing human heterotransplants (44), and its ability to induce apoptosis can be enhanced by inhibition of NF-κB (45). The differences in the efficiencies of inhibition of the Ras-Net pathway by docetaxel, vincristine, and CA4/XRP44X could be a consequence of them binding to different sites on tubulin. However, another colchicines-binding compound, nocodazole, did not inhibit the pathway efficiently.

In conclusion, this study shows that, among microtubule poisons, XRP44X and CA4 constitute an original class of drugs, which combine two anticancer clinically validated mechanisms: antimitotic and signaling pathway inhibitory activities (46).

Acknowledgments

Received 7/13/2007; revised 11/20/2007; accepted 1/3/2008.

Grant support: H. Zheng received fellowships from Sanofi-Aventis and EU FP6 Prima project 504587. The work in the Wasylyk laboratory was financed by Ligue Nationale Française contre le Cancer (Equipe labellisée), Ligue Régionale (Bas-Rhin) contre le Cancer, Ligue Régionale (Haut-Rhin) contre le Cancer, Association pour la Recherche contre le Cancer, Centre National de la Recherche Scientifique, Institut National de la Santé et de la Recherche Médicale, EU FP5 procure project QLK6-2000-00159 and FP6 Prima project 504587, INCa Axe IV and DKFZ-CGE projects, and AICR 05-390.

The costs of publication of this article were defrayed in part by the payment of page charges. This article must therefore be hereby marked *advertisement* in accordance with 18 U.S.C. Section 1734 solely to indicate this fact.

We thank Wasylyk laboratory members for support and encouragement, Doulaye Dembele for help with the IC_{50} determination, and the IGBMC core facilities.

References

1. McCormick F. Signalling networks that cause cancer. Trends Cell Biol 1999;9:M53–6.
2. Shaw RJ, Cantley LC. Ras, PI(3)K and mTOR signalling controls tumour cell growth. Nature 2006;441:424–30.
3. Bentires-Alj M, Kontaridis MI, Neel BG. Stops along the RAS pathway in human genetic disease. Nat Med 2006;12:283–5.
4. Roux PP, Blenis J. ERK and p38 MAPK-activated protein kinases: a family of protein kinases with diverse biological functions. Microbiol Mol Biol Rev 2004;68:320–44.
5. Tomlins SA, Mehra R, Rhodes DR, et al. TMPRSS2:ETV4 gene fusions define a third molecular subtype of prostate cancer. Cancer Res 2006;66:3396–400.
6. Tomlins SA, Rhodes DR, Perner S, et al. Recurrent fusion of TMPRSS2 and ETS transcription factor genes in prostate cancer. Science 2005;310:644–8.
7. Janknecht R. EWS-ETS oncoproteins: the linchpins of Ewing tumors. Gene 2005;363:1–14.
8. Ayadi A, Suelves M, Dolle P, Wasylyk B. Net, an Ets ternary complex transcription factor, is expressed in sites of vasculogenesis, angiogenesis, and chondrogenesis during mouse development. Mech Dev 2001;102:205–8.
9. Ayadi A, Zheng H, Sobieszczuk P, et al. Net-targeted mutant mice develop a vascular phenotype and up-regulate egr-1. EMBO J 2001;20:5139–52.
10. Zheng H, Wasylyk C, Ayadi A, et al. The transcription factor Net regulates the angiogenic switch. Genes Dev 2003;17:2283–97.
11. Buchwalter G, Gross C, Wasylyk B. The ternary complex factor Net regulates cell migration through inhibition of PAI-1 expression. Mol Cell Biol 2005;25:10853–62.
12. Buchwalter G, Gross C, Wasylyk B. Ets ternary complex transcription factors. Gene 2004;324:1–14.
13. Jordan MA, Wilson L. Microtubules as a target for anticancer drugs. Nat Rev Cancer 2004;4:253–65.
14. Honore S, Pasquier E, Braguer D. Understanding microtubule dynamics for improved cancer therapy. Cell Mol Life Sci 2005;62:3039–56.
15. Attard G, Greystoke A, Kaye S, De Bono J. Update on tubulin-binding agents. Pathol Biol (Paris) 2006;54:72–84.
16. Tron GC, Pirali T, Sorba G, Pagliai F, Busacca S, Genazzani AA. Medicinal chemistry of combretastatin a4: present and future directions. J Med Chem 2006;49:3033–44.
17. Criqui-Filipe P, Ducret C, Maira SM, Wasylyk B. Net, a negative Ras-switchable TCF, contains a second inhibition domain, the CID, that mediates repression through interactions with CtBP and de-acetylation. EMBO J 1999;18:3392–403.
18. Maira SM, Wurtz JM, Wasylyk B. Net (ERP/SAP2) one of the Ras-inducible TCFs, has a novel inhibitory domain with resemblance to the helix-loop-helix motif. EMBO J 1996;15:5849–65.
19. Dubs-Poterszman MC, Tocque B, Wasylyk B. MDM2 transformation in the absence of p53 and abrogation of the p107 G1 cell-cycle arrest. Oncogene 1995;11:2445–9.
20. Tsang M, Dawid IB. Promotion and attenuation of FGF signaling through the Ras-MAPK pathway. Sci STKE 2004;2004:pe17.
21. Ducret C, Maira SM, Lutz Y, Wasylyk B. The ternary complex factor Net contains two distinct elements that mediate different responses to MAP kinase signalling cascades. Oncogene 2000;19:5063–72.
22. Cruzalegui FH, Cano E, Treisman R. ERK activation induces phosphorylation of Elk-1 at multiple S/T-P motifs to high stoichiometry. Oncogene 1999;18:7948–57.
23. Ballif BA, Blenis J. Molecular mechanisms mediating mammalian mitogen-activated protein kinase (MAPK) kinase (MEK)-MAPK cell survival signals. Cell Growth Differ 2001;12:397–408.
24. Zhu WH, MacIntyre A, Nicosia RF. Regulation of angiogenesis by vascular endothelial growth factor and angiopoietin-1 in the rat aorta model: distinct temporal patterns of intracellular signaling correlate with induction of angiogenic sprouting. Am J Pathol 2002;161:823–30.
25. Kanthou C, Tozer GM. The tumor vascular targeting agent combretastatin A-4-phosphate induces reorganization of the actin cytoskeleton and early membrane blebbing in human endothelial cells. Blood 2002;99:2060–9.
26. Kanthou C, Greco O, Stratford A, et al. The tubulin-binding agent combretastatin A-4-phosphate arrests endothelial cells in mitosis and induces mitotic cell death. Am J Pathol 2004;165:1401–11.
27. Tozer GM, Kanthou C, Baguley BC. Disrupting tumour blood vessels. Nat Rev Cancer 2005;5:423–35.
28. Hadfield JA, Ducki S, Hirst N, McGown AT. Tubulin and microtubules as targets for anticancer drugs. Prog Cell Cycle Res 2003;5:309–25.
29. Ducret C, Maira SM, Dierich A, Wasylyk B. The net repressor is regulated by nuclear export in response to anisomycin, UV, and heat shock. Mol Cell Biol 1999;19:7076–87.
30. Yoon S, Seger R. The extracellular signal-regulated kinase: multiple substrates regulate diverse cellular functions. Growth Factors 2006;24:21–44.
31. Gundersen GG, Cook TA. Microtubules and signal transduction. Curr Opin Cell Biol 1999;11:81–94.
32. Cooney MM, Ortiz J, Bukowski RM, Remick SC. Novel vascular targeting/disrupting agents: combretastatin A4 phosphate and related compounds. Curr Oncol Rep 2005;7:90–5.
33. West CM, Price P. Combretastatin A4 phosphate. Anticancer Drugs 2004;15:179–87.
34. Pettit GR, Singh SB, Niven ML, Hamel E, Schmidt JM. Isolation, structure, and synthesis of combretastatins A-1 and B-1, potent new inhibitors of microtubule assembly, derived from *Combretum caffrum*. J Nat Prod 1987;50:119–31.
35. Ivetic A, Ridley AJ. Ezrin/radixin/moesin proteins and Rho GTPase signalling in leucocytes. Immunology 2004;112:165–76.
36. Kolch W. Coordinating ERK/MAPK signalling through scaffolds and inhibitors. Nat Rev Mol Cell Biol 2005;6:827–37.
37. Blagosklonny MV, Chuman Y, Bergan RC, Fojo T. Mitogen-activated protein kinase pathway is dispensable for microtubule-active drug-induced Raf-1/Bcl-2 phosphorylation and apoptosis in leukemia cells. Leukemia 1999;13:1028–36.
38. Okano J, Rustgi AK. Paclitaxel induces prolonged activation of the Ras/MEK/ERK pathway independently of activating the programmed cell death machinery. J Biol Chem 2001;276:19555–64.
39. Legrier ME, Oudard S, Judde JG, et al. Potentiation of antitumour activity of docetaxel by combination with trastuzumab in a human prostate cancer xenograft model and underlying mechanisms. Br J Cancer 2007;96:269–76.
40. Monje P, Hernandez-Losa J, Lyons RJ, Castellone MD, Gutkind JS. Regulation of the transcriptional activity of c-Fos by ERK. A novel role for the prolyl isomerase PIN1. J Biol Chem 2005;280:35081–4.
41. Bourgarel-Rey V, El Khyari S, Rimet O, et al. Opposite effects of antimicrotubule agents on c-myc oncogene expression depending on the cell lines used. Eur J Cancer 2000;36:1043–9.
42. Bourgarel-Rey V, Vallee S, Rimet O, et al. Involvement of nuclear factor κB in c-Myc induction by tubulin polymerization inhibitors. Mol Pharmacol 2001;59:1165–70.
43. Jung YJ, Isaacs JS, Lee S, Trepel J, Neckers L. Microtubule disruption utilizes an NF-κB-dependent pathway to stabilize HIF-1α protein. J Biol Chem 2003;278:7445–52.
44. McDaid HM, Lopez-Barcons L, Grossman A, et al. Enhancement of the therapeutic efficacy of taxol by the mitogen-activated protein kinase kinase inhibitor CI-1040 in nude mice bearing human heterotransplants. Cancer Res 2005;65:2854–60.
45. Bava SV, Puliappadamba VT, Deepti A, Nair A, Karunagaran D, Anto RJ. Sensitization of taxol-induced apoptosis by curcumin involves down-regulation of nuclear factor-κB and the serine/threonine kinase Akt and is independent of tubulin polymerization. J Biol Chem 2005;280:6301–8.
46. Sebolt-Leopold JS, Herrera R. Targeting the mitogen-activated protein kinase cascade to treat cancer. Nat Rev Cancer 2004;4:937–47.